VIP Core–Shell Catalysts

DOI: 10.1002/ange.201209799

# De Novo Design of Nanostructured Iron–Cobalt Fischer–Tropsch Catalysts

*V. Roberto Calderone, N. Raveendran Shiju, Daniel Curulla-Ferré, Stéphane Chambrey, Andrei Khodakov, Amadeus Rose, Johannes Thiessen, Andreas Jess, and Gadi Rothenberg**

Sustainable energy production (and consumption) is one of the key challenges of the 21st century. Energy demand is increasing steadily in the EU and in North America, and even faster in emerging economies, such as China and Brazil.[1] Major oil companies are considering alternative feedstocks, such as natural gas and biomass, promoting low-$CO_2$-footprint technologies. These developments are reviving the interest in the century-old Fischer–Tropsch synthesis (FTS).[2] Indeed, the last seven decades show a remarkably strong correlation between crude oil prices and research on FTS.[3] Currently, FTS technology is used for the production of ultraclean synthetic fuels in South Africa, Qatar, Malaysia, and China, starting from coal (so-called coal-to-liquids, or CTL) or natural gas (gas-to-liquids, GTL).[4]

Catalysis plays a critical part in nearly every large industrial process, and FTS is no exception. In FTS the active phase is usually made of iron or cobalt; the choice of which phase depending on various factors, such as the target product (fuels vs. chemicals) and cost.[5] These metals have complementary catalytic properties. Cobalt is chiefly used for converting 1:2 $CO:H_2$ syn-gas mixtures coming from natural gas. It gives higher conversion than iron as well as higher selectivity to paraffins.[6] Iron, a known water–gas-shift catalyst, is applied when the feed is CO-rich (as in biomass-derived syn-gas), thus helping to re-establish the optimal 1:2 stoichiometry. Cobalt-based catalysts represent the optimal choice for synthesizing middle distillate fuels, which is why the companies that commercialize FTS technology have chosen cobalt for all their projects aiming at the production of liquid fuels (Shell in Malaysia and Qatar, and Sasol in South Africa and Qatar). Cobalt-based catalysts have also been the choice of other companies with proprietary FTS technology including BP, ExxonMobil, Statoil, Oxford Catalysts, and CGTL. Compared to iron-based catalysts, cobalt-based catalysts exhibit higher stability, higher productivity, negligible effect of co-produced water, and higher resistance to attrition in slurry bubble column reactors.

Cobalt is recognized as a key metal. The European Commission, for example, has declared it as one of the 14 critical metals for the industrial and technological positioning of European industry.[7] But the cost factor of cobalt on such a large scale is a problem, since FTS reactors use hundreds of tons of catalyst. Moreover, state-of-the-art catalysts typically contain large cobalt particles, meaning that most of the metal atoms are not available for catalysis. Thus, the challenge is designing a cheaper catalyst that can be prepared on a very large scale, yet performs at least as well as pure cobalt. One of the most pronounced features of cobalt-based FTS catalysts is the particle-size dependence for both activity and selectivity.[8] The debate on the exact mechanism notwithstanding, many reports agree that the optimal catalyst particle size for producing diesel fractions at high conversion lies in the 5–10 nm range. Since both activity and selectivity are mainly driven by the active-phase topology, we decided to address the design of the active phase from a topological point of view: constraining the active phase on the outside (shell) of the particle and replacing the core with a cheaper material.[9] The problem is that the economic challenge comes hand-in-hand with a formidable chemical one. Gaining an economic advantage requires engineering of the particles at single-nanometer resolution, yet done in a manner that can be scaled up to multi-ton scale.

Figure 1 shows a price/performance simulation for various core/cobalt catalysts. The price of a core–shell material is a function of many parameters: precursor type, stoichiometry, density, and especially the relative size of core to shell. We see that a 50% saving, using any of the common Fe, Zn, Ti, or Si oxides, requires that the maximum shell radius must be only 10–20% of the particle radius. Even opting for the "larger" 10 nm particles, this means that the shell thickness should be only 1 nm. The challenge is therefore devising a catalyst synthesis method that can give cobalt shells just 1 nm thick, yet is simple and scalable. Herein we report the discovery of such a method and catalyst, as well as the characterization for this catalyst and its application in FTS.

The scale-up constraint rules out all routes that require high sophistication, extreme temperatures, or expensive chemicals. Instead, we chose a classic coating method: surface nucleation of a cobalt phase onto iron oxide colloids. Rather appropriately, considering the age of the FTS process, we are

[*] Dr. V. R. Calderone, Dr. N. R. Shiju, Prof. Dr. G. Rothenberg
Van't Hoff Institute for Molecular Sciences, University of Amsterdam
Science Park 904, 1098 XH, Amsterdam (The Netherlands)
E-mail: g.rothenberg@uva.nl
Homepage: http://hims.uva.nl/hcsc
Dr. D. Curulla-Ferré
Gaz & Energies Nouvelles, Total S.A.
Paris La Defense 6 (France)
Dr. S. Chambrey, Prof. A. Khodakov
Unité de Catalyse et de Chimie du Solide (UCCS), Université des Sciences et Technologies de Lille 1, Cité Scientifique
Bâtiment C3–BP48, 59651 Villeneuve d'Ascq Cedex (France)
A. Rose, J. Thiessen, Prof. Dr. A. Jess
Department of Chemical Engineering, Center of Energy Technology, University of Bayreuth
Universitätstrasse 30, 95440 Bayreuth (Germany)

Supporting information for this article is available on the WWW under http://dx.doi.org/10.1002/anie.201209799.

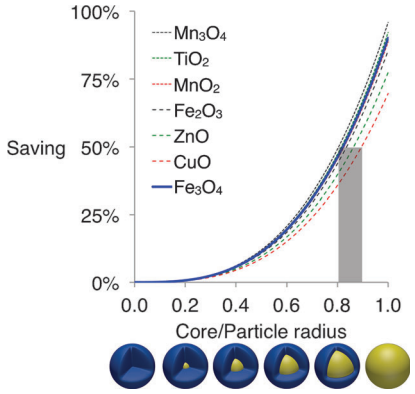


***Figure 1.*** Multi-parameter simulation showing the comparative cost of spherical core–shell catalysts with various metal oxide cores and cobalt shells. Each curve is based on the data for a specific oxide (bulk price, density, metal/oxygen stoichiometry, precursor stoichiometry, and precursor density), showing the percentage of cost reduction when the core of a pure cobalt particle is replaced with a given oxide at a given radius. The spheres below the abscissa show the relative core:shell sizes.

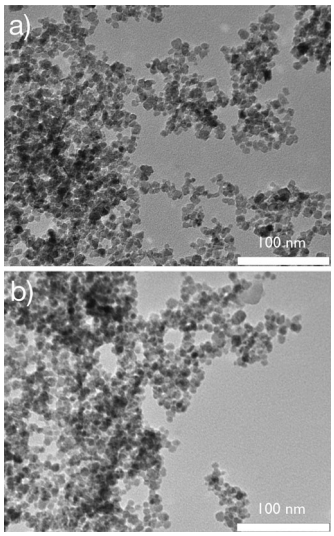


***Figure 2.*** TEM pictures showing a) cobalt oxide particles precipitated from a 50 mL suspension containing 10 mL of NaOH 10 M and 20 g $L^{-1}$ magnetite particles, by slow addition of 10 mL of a $CoNO_3$ $H_2O$ solution. Final Co/Fe = 60 wt%; b) parent magnetite particles with mean particle size of 7 nm.

revisiting the method that recording-tape industries, such as 3M, BASF, and TDK used in the 1960s for producing magnetic tapes.[10] Polymer-based tapes containing cobalt-doped acicular iron oxide particles were the standard recording material used in the production of compact cassettes.[11]

We have now been able to optimize this process to produce the spherical nanoparticles required for FTS instead of the high aspect ratio particles used in magnetic tapes. The result is a method that is cheap, reliable, efficient and, most importantly, scalable for synthesizing spherical core–shell particles with a magnetite core and a cobalt oxide shell. It enables the tuning of the shell thickness to within ±1.0 nm. The synthesis is a two-step process. First, 7 nm magnetite particles were synthesized by a slightly modified Massart method.[12] In a typical synthesis, $FeCl_3{\cdot}x\,H_2O$ and $FeCl_2{\cdot}x\,H_2O$ were mixed together in $H_2O$. Then, $NH_4OH$ (29%) was added, and magnetite formation was visible as a black precipitate. The particles were settled using a magnet and the supernatant was discharged. The magnetite particles were re-dispersed in 2 M $HNO_3$ and stirred. After 10 min the particles were settled with a magnet. The supernatant was removed, and the particles were peptized with water. Then, the magnetite suspension was mixed with a 10 M NaOH solution. The mixture was heated up to 60–70 °C. Then a $Co(NO_3)_2{\cdot}x\,H_2O$ solution was slowly added to the magnetite suspension. The cobalt concentration in the solution was chosen to achieve a final 60 wt% Co/Fe ratio. The reaction was kept at 60–70 °C for 2 h. After cooling to room temperature, the precipitate was washed with water, removing any trace of $Na^+$ (a possible catalyst poison).

We focused our attention on the magnetite sample with mean particle size of 7 nm and its derivatives, as this size range is recognized as optimal for cobalt-based FTS catalysts. We expected the coating process to only affect the small particles because of their higher surface energy and surface area; for this reason the particle size did not increase significantly after coating, even upon addition of 60 wt% cobalt over iron (Figure 2).

Among the samples with different Co/Fe ratios, the one with the highest cobalt content is best suited for giving visual evidence of the core–shell structure. In the HRTEM shown in

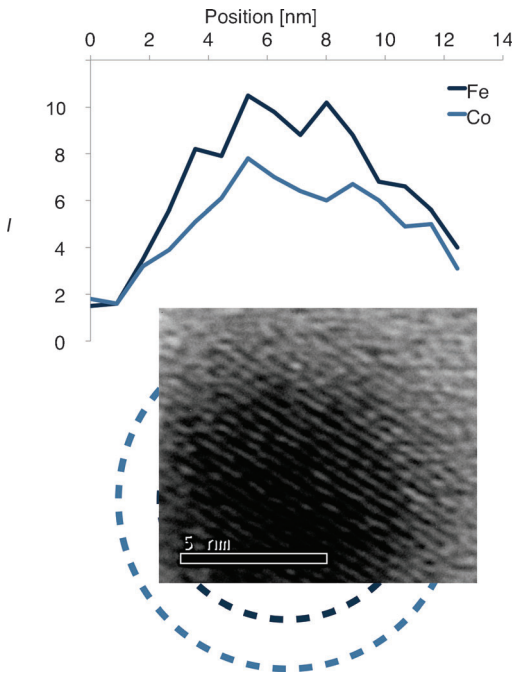


***Figure 3.*** HRTEM picture showing the inner structure of a core–shell particle. A core and a shell can be distinguished by different contrast (blue broken lines are drawn for clarity). The lattice fringes (seen as diagonal lines) through the whole particle suggest an epitaxial growth formation mechanism. The graph gives numerical support (based on EDX data) to the nanostructure description: the cobalt concentration in the shell is higher than in the core.

Figure 3, the nanostructure of the particles is visible. The core and the shell have different contrasts, revealing a different chemical composition and, as quantified by energy dispersive X-ray spectroscopy (EDX), an iron-based core coated with

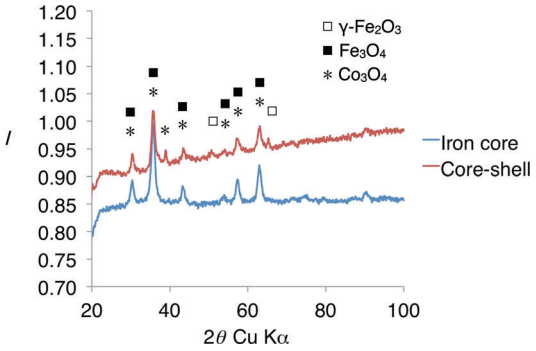


***Figure 4.*** Powder XRD patterns of the iron oxide particles (core) and of the core–shell particles. Core and shell are isostructural. Small quantities of $\gamma$-$Fe_2O_3$ are detected, probably as a result of partial oxidation of the iron-based core during the coating process.

a cobalt-rich shell. Furthermore, lattice fringes run across the whole particle body. This feature suggests that epitaxial growth is the predominant mechanism for the formation of this core–shell material, as confirmed by the X-ray diffraction (XRD) characterization (Figure 4): the diffraction patterns of the $Fe_3O_4$ core and the core–shell material can be superimposed perfectly (except for a small amount of oxidized iron oxide produced during the coating process).

No matter how well prepared a material is, an active phase alone is never a catalyst. Before testing it, we had to overcome two sets of problems, namely how to support the material and how to retain the core–shell structure upon activation. The supporting procedure was kept as simple as possible: the core–shell particles were first mixed with nano-sized alumina particles (Aeroxide Alu C, specific surface area (BET) = 100 $m^2g^{-1}$; particle size = 13 nm). Then, a slurry was formed by adding the minimum amount of water. This slurry was then dried at room temperature and resulting pellets crushed and sieved to the desired size for catalytic testing. The interaction between the active phase and the support was established directly during the activation (reduction) step, thus avoiding any unnecessary thermal treatment that could destroy the core–shell nanostructure. Temperature programmed reduction (TPR) suggests that by properly selecting the reduction temperature (in this case, $T < 400\,^{\circ}C$, see Supporting Information) the cobalt shell can be selectively reduced to its metal form: the core–shell structure is retained and the only active phase is cobalt.

These core–shell materials were tested in two types of FTS lab-scale reactors (see details in the Supporting Information) and were shown to be efficient as FTS catalysts. First, we tested the stability of the catalysts using a small-scale setup (0.2 $L\,h^{-1}$, $m_{cat} = 0.03$ g, $T = 240\,^{\circ}C$, $P = 20$ bar, space velocity (SV) = 111 $mL\,min^{-1}\,g^{-1}$). The core–shell catalysts were more stable than the iron parent samples. After 90 h on stream, the core–shell catalyst retained 100% of its maximum highest

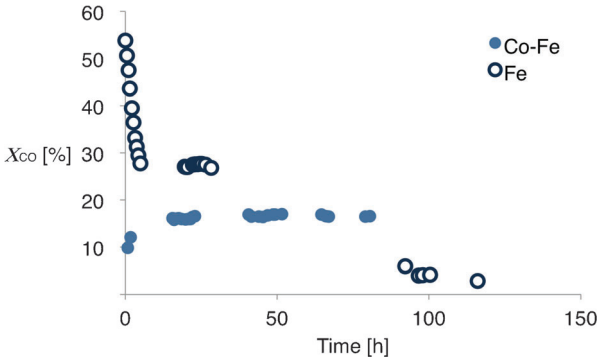


***Figure 5.*** Catalytic activity (measured in a small-scale fixed-bed reactor, SV = 111 $mL\,min^{-1}/g_{cat}$) expressed in terms of CO conversion. The different stability of the two catalysts with time on stream is shown. The iron-based catalyst shows a higher starting activity, but loses 50% of its activity after just 10 h. It becomes almost inactive after 90 h. Conversely, the core–shell catalyst, although less active, retains the activity throughout the duration of the test.

activity ($X_{CO} = 16\%$, reached after 10 h on stream, see Figure 5). Importantly, these catalysts also show a methane selectivity of 18%, leaving room for more than 80% of valuable hydrocarbons.

We ran larger scale experiments using a reactor with a feed of 20 $L\,h^{-1}$, $m_{cat} = 4$ g, SV = 83 $mL\,min^{-1}\,g^{-1}$ (full experimental details are given in the Supporting Information). As Table 1 shows, the core–shell catalyst gave approx-

***Table 1:*** Selectivity values ($X_{CO} = 20\%$) for the core–shell catalyst at larger scale ($m_{cat} = 4$ g, SV = 83 $mL\,min^{-1}\,g^{-1}$).

| $X_{CO}$ | Selectivity | | | | | Alkane/alkene |
|---|---|---|---|---|---|---|
| | $CH_4$ | $CO_2$ | oxy.[a] | alkene | $C_5$–$C_{27}$ | |
| 20% | 18% | 2% | 10% | 20% | 40% | 2.5 $g\,g^{-1}$ |

[a] oxy = oxygenates.

imately 40% selectivity to $C_5$–$C_{27}$ at 20% CO conversion. This test, which was performed under realistic FTS conditions, (230 °C and 32 bar) shows the industrial potential of this catalyst.

Analyzing the catalyst performance with a focus on the product distribution gives further insight (Table 1). Two chain-growth probability factors ($\alpha$) can be calculated (Figure 6): one for the light fraction (0.49) and another for the heavy fraction (0.78). Furthermore, the catalyst showed a high selectivity towards alkenes (ca. 20%) as well as oxygenates (ca. 10%), but the oxygenates showed a low growth probability factor, $\alpha = 0.55$. These facts suggest that iron is interfering with the activity of the catalyst.

Two main possibilities arise: 1) iron is interacting with cobalt and changing the electronic and/or the crystal structure of the shell; among the number of phases cobalt can crystallize, hcp and fcc structures are recognized as the most active towards FTS. In bimetallic systems with iron, cobalt retains its fcc/hcp structure for low iron concentrations. At higher concentration, iron imposes a bcc crystal structure on

  

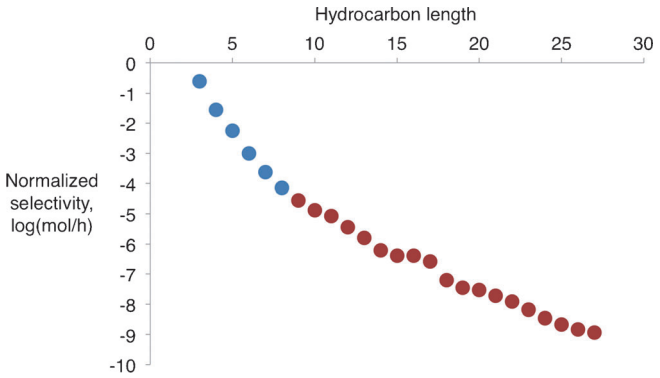


***Figure 6.*** Selectivity of the core–shell catalyst is represented as the carbon-number-based normalized selectivity on a logarithmic scale for a conversion value of $X_{CO} = 20\%$. Two different regimes can be observed: a low chain growth probability for the range $C_{3-8}$ (blue), and a high chain growth probability for $C_{8+}$ (red).

cobalt, thus affecting the activity and selectivity of the catalyst.[5d] It was shown by Duvenhage et al. that if the structure of the catalyst is completely driven by iron, then iron–cobalt catalysts have lower activity than pure cobalt materials and that the selectivity resembles that of our core/shell catalyst.[5d] 2) a partial restructuring of the core–shell particles takes place, with surface enriching of iron at the expense of cobalt. However, iron segregation is more relevant at low iron concentrations.[5d,13] Note that, even if restructuring occurs, we see only 2% $CO_2$. This result shows that iron on the surface is not promoting the water–gas-shift reaction. Rather, we see a cooperative effect between the two metals.

A more detailed comparison with published works is problematic. Because of the high number of parameters involved in the process and the typical restructuring of FTS catalysts on stream, every catalyst (and often every FTS setup) is unique.[14] However, we can say that the core–shell Fe–Co catalysts give sufficiently low $CO_2$ and methane and sufficiently high alkenes and gasoline/diesel fractions to merit industrial interest.[15]

In summary, with the specific goal of preparing a FTS catalyst, we developed a new method that gives supported spherical core–shell materials with an iron core and a cobalt shell and ensures their core–shell structure is retained upon activation. The synthesis method is cheap and scalable to the multi-ton scale required. The materials proved to be efficient FTS catalysts. An efficient particle design suggests confining the active, more expensive phase on a thin shell grown on a cheaper core of the proper size. Herein we have reported a new approach to address the efficient preparation of size-dependent performance catalysts.

## *Experimental Section*

The synthesis of core–shell iron/cobalt particles is a two-step process. First 5–15 nm magnetite particles were synthesized by a slightly modified Massart method. In a typical synthesis, $FeCl_3{\cdot}x\,H_2O$ (9.02) and $FeCl_2{\cdot}x\,H_2O$ (3.26 g) were mixed together in $H_2O$ (380 mL) and $NH_4OH$ (29%; 15 to 30 mL) was added: magnetite formation was visible as a black precipitate. The particles were washed with $H_2O$ (300 mL) many times until the pH value of the supernatant was constant. The magnetite particles were then peptized with a 2 M $HNO_3$ solution (40 mL) . The precipitate was recovered with a magnet and redispersed in water. 20 g $L^{-1}$ magnetite suspension (50 mL) was mixed with a 10 M NaOH solution (10 mL). The mixture was heated to 70 °C and a $Co(NO_3)_2{\cdot}x\,H_2O$ solution (10 mL) slowly added to the magnetite suspension at the speed of 0.2 mL $min^{-1}$. The Co concentration in the solution was chosen to achieve a final Co/Fe wt% varying in the 3–60 wt% range. The reaction was kept at 60–70 °C for 2 h. After cooling to room temperature, the precipitate was washed with water, (removing any trace of $Na^+$) and the supernatant solution was removed and the remaining slurry freeze-dried. The core–shell particles were successively mixed with nanosized alumina powder (average size 13 nm) to obtain a 20 wt% cobalt-based catalyst, and a slurry was prepared by adding the minimum amount of water. TEM and HRTEM/EDX characterization was performed on a TECNAI 12 and TECNAI 20, respectively. Extensive description of the different reactors used for the FTS tests is given in the Supporting Information.

Received: December 7, 2012
Published online: February 28, 2013

**Keywords:** cobalt · Fischer–Tropsch synthesis · heterogeneous catalysis · nanoparticles · synthetic fuels

[1] International Energy Agency, "World Energy Outlook" can be found under http://www.worldenergyoutlook.org/media/weowebsite/2008-1994/WEO2008.pdf, **2008**.
[2] F. Fischer, H. Tropsch, *Ber. Dtsch. Chem. Ges.* **1923**, *56*, 2428–2443.
[3] E. de Smit, B. M. Weckhuysen, *Chem. Soc. Rev.* **2008**, *37*, 2758–2781.
[4] A. Steynberg, M. Dry, *Fischer–Tropsch Technology*, *Vol. 152*, Elsevier, Dordrecht, **2004**.
[5] a) D. J. Duvenhage, N. J. Coville, *Appl. Catal. A* **1997**, *153*, 43–67; b) D. J. Duvenhage, N. J. Coville, *Appl. Catal. A* **2002**, *233*, 63–75; c) D. J. Duvenhage, N. J. Coville, *J. Mol. Catal. A* **2005**, *235*, 230–239; d) D. J. Duvenhage, N. J. Coville, *Appl. Catal. A* **2005**, *289*, 231–239; e) H. Arai, K. Mitsuishi, T. Seiyama, *Chem. Lett.* **1984**, 1291–1294; f) X. Ma, Q. Sun, F. Cao, W. Ying, D. Fang, *J. Nat. Gas Chem.* **2006**, *15*, 335–339; g) A. Tavasoli, M. Trépanier, R. M. M. Abbaslou, A. K. Dalai, N. Abatzoglou, *Fuel Process. Technol.* **2009**, *90*, 1486–1494; h) S. Lögdberg, D. Tristantini, O. Borg, L. Ilver, B. Gevert, S. Jaras, E. A. Blekkan, A. Holmen, *Appl. Catal. B* **2009**, *89*, 167–182.
[6] A. Y. Khodakov, *Catal. Today* **2009**, *144*, 251–257.
[7] European Commission, "Critical raw materials for the EU" can be found under http://ec.europa.eu/enterprise/policies/raw-materials, **2010**.
[8] G. L. Bezemer, J. H. Bitter, H. P. C. E. Kuipers, H. Oosterbeek, J. E. Holewijn, X. Xu, F. Kapteijn, A. J. van Dillen, K. P. de Jong, *J. Am. Chem. Soc.* **2006**, *128*, 3956–3964.
[9] a) L. Durán Pachón, M. B. Thathagar, F. Hartl, G. Rothenberg, *Phys. Chem. Chem. Phys.* **2006**, *8*, 151–157; b) S. H. Joo, J. Y. Park, C.-K. Tsung, Y. Yamada, P. Yang, G. A. Somorjai, *Nat. Mater.* **2009**, *8*, 126–131; c) S. Wei, Q. Wang, J. Zhu, L. Sun, H. Lin, Z. Guo, *Nanoscale Res. Lett.* **2011**, *3*, 4474–4502.
[10] a) Y. Tokuoka, S. Umeki, Y. Kubota (TDK Electronic Company), US3953656, **1976**; b) W. D. Haller, R. M. Colline (Minnesota Mining and Manufacturing), US3573980, **1971**; c) T. M. Kanten (Minnesota Mining and Manufacturing), US4226909, **1980**; d) A. Lehner, H. Hartmann, R. Bachman, W. Balz, A. Kohl (BASF), US4328282, **1982**.
[11] a) G. Bate, *J. Magn. Magn. Mater.* **1991**, *100*, 413–424; b) Y. Imaoka, S. Umeki, Y. Kubota, Y. Tokuoka, *IEEE T. Magn.* **1978**, *14*, 649–654; c) L. Neel, (Societe d'Electro-Chimie, d'Electro-

  

Metallurgie et des AcieriesElectriques d'Ugine), US2463413, **1949**; d) K. Sakai, H. Saguchi, T. Nishimura, *J. Appl. Crystallogr.* **2001**, *34*, 102 – 107.

[12] R. Perzynski, D. Salin, V. Cabuil, R. Massart, *IEEE T. Magn.* **1986**, *MAG-17*, 1247 – 1248.

[13] O. de la Peña O'Shea, M. Álvarez-Galván, J. Campos-Martín, J. Fierro, *Appl. Catal. A* **2007**, *326*, 65 – 73.

[14] V. R. Calderone, N. R. Shiju, D. Curulla-Ferré, G. Rothenberg, *Green Chem.* **2011**, *13*, 1950 – 1959.

[15] V. R. Calderone, N. R. Shiju, G. Rothenberg, D. Curulla-Ferré (Total SA), WO2012163969, **2011**.